

Methane emissions responsible for record-breaking atmospheric methane growth rates in 2020 and 2021

Liang Feng¹, Paul I. Palmer^{1,2,*}, Robert J. Parker^{3,4}, Mark F. Lunt², Hartmut Bösch^{3,4}

1 National Centre for Earth Observation, University of Edinburgh, Edinburgh, UK

2 School of GeoSciences, University of Edinburgh, Edinburgh, UK

3 National Centre for Earth Observation, Space Park Leicester, University of Leicester, UK

4 Earth Observation Science, School of Physics and Astronomy, University of Leicester, UK

10 *Correspondence to:* Paul I. Palmer (paul.palmer@ed.ac.uk)

Abstract. The global atmospheric methane growth rates reported by NOAA for 2020 and 2021 are the largest since systematic measurements began in 1983. To explore the underlying reasons for these anomalous growth rates we use newly available methane data from the Japanese Greenhouse gases Observing SATellite (GOSAT) to estimate methane surface emissions. Relative to baseline values in 2019 we see the largest annual increases in methane emissions during 2020 over Eastern Africa (13±3 Tg), tropical Asia (4±3 Tg), tropical South America (3±3 Tg), and temperate Eurasia (3±3 Tg), and the largest reductions over China (-6±2 Tg) and India (-2±2 Tg). We find comparable emission changes in 2021, relative to 2019, except for tropical and temperate South America where emissions increased by 9±3 Tg and 5±3 Tg, respectively, and tropical Asian emissions increased by 8±2 Tg. The elevated contributions we saw in 2020 over the western half of Africa (-5±3 Tg) and Europe (-3±3 Tg) are substantially reduced in 2021, compared to our 2019 baseline. We find statistically significant positive correlations between anomalies of tropical methane emissions and groundwater, consistent with recent studies that have highlighted a growing role for microbial sources over the tropics. Emission reductions over India and China are expected in 2020 due to the Covid-19 shutdown but continued in 2021, which we do not currently understand. Based on a range of sensitivity studies for which we assume different spatial and temporal distributions of OH reduction in 2020, due to reduced pollutant emissions during the Covid-19 shutdown, and on our results from an inversion that includes OH scaling factors, we find that our *a posteriori* emissions in 2020 are 22-30% lower than our control calculation. We conclude therefore that most of the observed increase in atmospheric methane during 2020 and 2021 is due to increased emissions rather than reduced levels of OH.

1 Introduction

The atmospheric growth rate of methane in the 21st century has defied a definitive explanation: following a period of near-zero growth during 2000-2007 (Rigby et al. 2008) growth rates have accelerated, with values reported by NOAA for 2020 (15.29±0.38 ppb) and 2021 (16.94±0.38 ppb) exceeding all prior values since their records began in 1983. The underlying

reasons for these anomalous growth rates in 2020 and 2021 are currently subject to intense debate with some studies attributing most of the growth in 2020 to a reduction in the hydroxyl radical (OH) sink of methane due to global-scale reductions in nitrogen oxides due to pandemic-related industry shutdowns (Laughner et al. 2021). On the face of it, this appears to be a reasonable explanation, but recent studies have used satellite observations of atmospheric methane to reveal regional hotspots over the tropics that are responding to changes in climate and have global significance (Pandey et al. 2021; Lunt et al. 2019; 2021; Pandey et al. 2017; Feng, Palmer, Zhu, et al. 2022; Palmer et al. 2021; Wilson et al. 2020). Here, we use satellite observation of methane from the Japanese Greenhouse gases Observing SATellite (GOSAT) to document global and regional changes in emissions, extending a recent study (Feng, Palmer, Zhu, et al. 2022). In the next section we describe the data and methods used to infer methane emissions. In section 3 we describe our results and conclude the study in section 4.

40 **2 Data and Methods**

We follow closely the methodology from a recent study (Feng, Palmer, Zhu, et al. 2022) in which we simultaneously infer methane and CO₂ fluxes in 2020 and 2021 by directly assimilating proxy GOSAT XCH₄:XCO₂ retrievals (X denotes atmospheric column-averaged dry-air mole fraction). These data are anchored by surface methane and CO₂ measurements from an *in situ* observation network. The main advantage of this approach is that it does not rely on assumed model CO₂ concentrations to extract XCH₄ from the proxy ratio. For the sake of brevity, we include only details relevant to the calculations shown here.

2.1 GOSAT methane proxy data

We use version 9.0 of the proxy GOSAT XCH₄:XCO₂ retrievals from the University of Leicester (R. J. Parker et al. 2020; R. Parker and Boesch 2020), including both nadir observations over land and glint observations over the ocean. Analyses have shown that these retrievals have a bias of 0.2%, with a single-sounding precision of ~0.72%. We globally remove a slightly larger 0.3% bias from the GOSAT proxy data to improve the comparison with independent *in situ* observations (Feng et al. 2017; Feng, Palmer, Parker, et al. 2022). We assume that each single GOSAT proxy XCH₄:XCO₂ ratio retrieval has an uncertainty of 1.2% to account for possible model errors, including the errors in atmospheric chemistry and transport, which helps to prevent model overfitting to observations.

55 **2.2 *In situ* data**

To anchor the GOSAT proxy ratio observations (Fraser et al. 2014b), we also ingest simultaneously the CO₂ and methane mole fraction data at surface-based sites, chosen from the NOAA compilation of the multi-laboratory *in-situ* measurements (Di Sarra et al. 2021; 2022; Cox et al. 2021; 2022). We include the same subset of the surface sites used by a recent study that documented year to year variations of methane emissions during 2010-2019 (Feng, Palmer, Zhu, et al. 2022). We assume uncertainties of 0.5 ppm and 8 ppb for these *in situ* observations of CO₂ and methane respectively (Feng, Palmer, Zhu, et al. 2022).

2.3 GEOS-Chem atmospheric chemistry transport model

We use the GEOS-Chem model of atmospheric chemistry and transport at a horizontal resolution of 2° (latitude) \times 2.5° (longitude), driven by the MERRA2 meteorological reanalyses from the Global Modeling and Assimilation Office Global Circulation Model based at NASA Goddard Space Flight Center.

Our CO₂ and methane model calculations are described in recent study (Feng, Palmer, Zhu, et al. 2022). The *a priori* CO₂ flux inventory includes monthly biomass burning emission (van der Werf et al. 2017); monthly fossil fuel emissions for 2019 in the absence of more recent data (Oda and Maksyutov 2021); monthly climatological ocean fluxes (Takahashi et al. 2009); and 3-hourly terrestrial biosphere fluxes (Randerson et al. 1996).

The *a priori* methane fluxes from nature include monthly wetland emissions, including rice paddies (Bloom et al. 2017); monthly fire methane emissions (van der Werf et al. 2017); and termite emissions (Fung et al. 1991). We include emissions from geological macroseeps (Kvenvolden and Rogers 2005; Etiope 2015). For *a priori* anthropogenic emissions we use the EDGAR v4.32 global emission inventory for 2012 (Janssens-Maenhout et al. 2019) that includes various sources related to human activities (e.g., oil and gas industry, coal mining, livestock, and waste).

We use monthly 3-D fields of OH, consistent with observed values for the lifetime of methyl chloroform, from the GEOS-Chem full chemistry simulation (Mao et al. 2013; Turner et al. 2015) to describe the main oxidation sink of methane. Using pre-computed fields of OH greatly simplifies our calculations, but in sensitivity calculations described below we examine the sensitivity of our results to different OH distributions. We also include net microbial consumption of methane in soil (Fung et al. 1991) and reaction with chlorine atoms (Thanwerdas et al. 2019).

To explore the sensitivity of our methane emission estimates for 2020 due to inferred reductions in OH due to large-scale industrial shutdown due to Covid-19 (Cooper et al. 2022), we scale down our baseline monthly 3-D OH fields by 5% where combustion emissions of CO₂ (Oda and Maksyutov 2021) were larger than the mean emissions over Africa, resulting in reductions mainly between 15°N and 65°N . Our choice of 5% represents a reduction based on a recent study (Laughner et al. 2021). A recent study that accounted for reductions in nitrogen oxide emissions estimated a global OH reduction of $\sim 4\%$ due to Covid-19 lockdowns in 2020 (Miyazaki et al. 2021), which showed strong spatial and temporal variations, with localized reductions peaking at 20-30%. In the absence of direct measurements of OH and without considering co-reductions in non-methane hydrocarbons, these (and similar) results have large uncertainties. To further examine the impact of reduced OH levels on the atmospheric growth of methane during 2020, we have reported in Appendix D the results of two additional experiments that assumed different distributions of the OH reduction, guided by observed changes in tropospheric ozone (Ziemke et al.

2022). In Appendix E we report results from simultaneously inferring large-scale OH changes and methane emissions from atmospheric methane observations. These additional results are summarized in section 3.

2.4 Ensemble Kalman filter inverse method

We use an ensemble Kalman Filter (EnKF) framework to estimate simultaneously CO₂ and methane fluxes from satellite measurements of the atmospheric CO₂ and methane (Feng, Palmer, Zhu, et al. 2022). Our state vector includes monthly scaling factors for 487 regional pulse-like basis functions (Figure A1) that describe CO₂ and methane fluxes, including 476 land regions and 11 oceanic regions. We define these land sub-regions by dividing the 11 TransCom-3 land regions into 42 nearly equal sub-regions, with the exception for temperate Eurasia that has been divided into 56 sub-regions due to its large landmass. We use the 11 oceanic regions defined by the TransCom-3 experiment. We use a 4-month moving lag window to reduce the computational costs for projecting the flux perturbation ensemble into observation space long after (>4 months) their emissions, beyond which time it is difficult to distinguish between the emitted signal from variations in the ambient background atmosphere (Fraser et al. 2014a; Feng et al. 2017). Our *a priori* fluxes are described above. For simplicity we assume a fixed uncertainty of 40% for coefficients corresponding to the *a priori* CO₂ fluxes over each sub-region, and a larger uncertainty (60%) for the corresponding methane emissions. We also assume that *a priori* errors for the same gas are correlated with a spatial correlation length of 300 km and with a temporal correlation of one month.

As a sensitivity test, we also report methane fluxes inferred using the same EnKF approach but using the proxy GOSAT XCH₄ data and *in situ* methane data. These GOSAT XCH₄ retrievals are calculated from the XCH₄:XCO₂ ratio by applying an ensemble mean of model XCO₂, and then bias-corrected according to comparison with TCCON XCH₄ retrievals (R. J. Parker et al. 2020).

2.5 Correlative data

To help interpret the changes in methane emission estimates we use additional datasets that are relevant to microbial or pyrogenic production of methane. We use monthly surface temperature fields at a spatial resolution of 2°x2.5° from the Modern-Era Retrospective Analysis for Research and Applications, version 2 (MERRA2) developed by the Global Modeling and Assimilation Office, NASA Goddard Space Flight Center (Bosilovich *et al.*, 2015). Precipitation data are taken from the NOAA CMAP (CPC Merged Analysis of Precipitation) long-term global rainfall dataset (Xie and Arkin 1997) that provides near-global monthly coverage at a spatial resolution of 2.5° × 2.5°, from 1979 to near-present. In addition, we use monthly total water storage (liquid water equivalent depth, LWE) on a 1° × 1° global grid from the NASA/DLR Gravity Recovery and

Climate Experiment Follow-on (GRACE-FO) (Landerer et al. 2020). Finally, we explore monthly biomass burning emissions from the Global Fire Emissions Database (GFED v4) (van der Werf et al. 2017).

2 Results

125 Table 1 summarizes our global emission estimates inferred from GOSAT for 2020 and 2021; and for 2019, which we use as our baseline year throughout this study (Figure A2). The largest change in our global *a posteriori* emissions occurs during 2019—2020 (27 Tg) from 583.7 to 610.7 Tg/yr. Our *a posteriori* emission estimates for 2019 and 2020 are within 2% of values reported by an independent study (Qu et al. 2022), consistent with our reported uncertainties. These elevated emissions are sustained, but not further increased, during 2021 (609.5 Tg/yr).

130

The 27 Tg emission increase in 2020 and the lack of further emissions growth in 2021 may appear inconsistent with the NOAA global annual mean growth rates of 15.3 and 16.9 ppb in 2020 and 2021, respectively (Table 1). Based on these reported atmospheric growth rates, and after considering the effects of methane sinks, we find that a one-box model calculation predicts an increase in emissions of 12.6 Tg between 2019 and 2020 and a further 15.1 Tg increase in 2021 (see Appendix B and Figure 135 B1). These calculations use annual mean values that effectively represent the emissions increase between the middle of each successive year rather than the beginning and end. After considering the increases in monthly mean NOAA data, we find that the simple box model predicts a similar increase in emissions between December 2019 (583 Tg yr⁻¹) and December 2020 (610 Tg yr⁻¹) of 27 Tg yr⁻¹, with emissions thereafter stabilizing, with mean emissions of 610 Tg yr⁻¹ in 2021. As such, we conclude that the global mean emission results inferred from GOSAT are consistent with those inferred from NOAA surface data, 140 assuming a fixed methane atmospheric lifetime.

Figure 1 shows the broad geographical breakdown for our reported global changes in methane emissions. Relative to 2019, we find widespread increased emissions during 2020 except for China and India. Relative to baseline values in 2019 we see the largest annual increases in methane emissions during 2020 over Eastern Africa (13±3 Tg), tropical Asia (4±3 Tg), tropical 145 South America (3±3 Tg), and temperate Eurasia (3±3 Tg), and the largest reductions over China (-6±2 Tg) and India (-2±2 Tg). Emission changes relative to 2019 are comparable in 2021, except for tropical and temperate South America increases to 9±3 Tg and 5±3 Tg, respectively, and tropical Asia increases to 8±2 Tg. The elevated contributions we saw in 2020 over the western half of Africa (-5±3 Tg) and Europe (-3±3 Tg) are substantially reduced in 2021, compared to our 2019 baseline. This is broadly consistent with a recent study that showed that methane emissions inferred from TROPOMI were significantly 150 higher in the first half of 2020 than during 2019 (McNorton et al. 2022). This study focused mainly on major countries, while we find the largest changes are over tropical latitudes where emissions in the second half of 2020 make significant contributions (Figure A3).

Figure 2 shows the distribution of methane emissions from 2020 and 2021 and the relative changes from 2019 (Figure A1).
155 During 2020, there are significant decreases (20-30%) over the manufacturing regions such as eastern China, India, central
America, and eastern Europe. There are also significant increases across eastern Africa (30-40%), eastern North America
(30%), and maritime Southeast Asia (30%). During 2021, we see similar changes in emissions, but they are typically
exaggerated. There is more of a pronounced increase over East Africa (>50%), southern Brazil (50%), and eastern North
America (up to 40%), and large decreases over eastern China (-50%) and western Russia (-50%). During 2021 there is also a
160 large decrease over equatorial West Africa and eastern Europe (Figure 1). There are substantial seasonal changes in methane
emissions (Figure A3) that are broadly consistent with seasonal changes in temperature and rainfall (not shown).

Figure 3 shows different annual surface temperature warming patterns in 2020 and 2021. During 2020 the high northern
latitudes are dominated by summer warming over Siberia (2-3 K on an annual scale) that has been linked to greenhouse gas
165 emissions (Ciavarella et al. 2021) and surface temperatures over Alaska were 2-3 K cooler than baseline values in 2019, where
there were comparatively small changes in groundwater (< 5 cm). North America, western Europe and Scandinavia also
experienced anomalously warm annual mean temperatures (typically within ± 2 K of 2019 values). There were smaller changes
in temperatures at low latitudes (typically ± 1 K of 2019 values), but larger increases in groundwater (± 10 -20 cm) associated
with higher changes in rainfall (Figure A4), particularly over East Africa and eastern Brazil. During 2021, high northern
170 latitudes were cooler than 2019 (<2-3 K) except for the contiguous US and Canada (higher than 2019 values by 2-3 K).
Midlatitudes and low latitudes generally did not experience the warm temperatures of 2020. Elevated groundwater was
sustained in 2021 over East and Southern Africa, eastern tropical South America (principally Brazil but stretching up to
Venezuela), central America, India, maritime Southeast Asia, and north and southeast Australia. Groundwater decreased over
the contiguous US, part of tropical South America and parts of Eurasia. We find generally stronger annual and seasonal
175 relationships between methane emission anomalies and hydrological anomalies (rainfall and groundwater) for 2020 and 2021
(Figure A5) than for temperature anomalies. Particularly, we find statistically significant large-scale positive correlations
(typically 0.5-0.6; $p < 0.001$) for all seasons between methane and groundwater anomalies over Eastern Africa, tropical South
America, and tropical Asia, but no significant correlation between methane and surface temperature anomalies. This is
consistent with recent studies that have highlighted an increasing role for microbial sources in the tropical methane budget
180 (Lunt et al. 2019; Feng, Palmer, Zhu, et al. 2022; Wilson et al. 2020). Over North America, we find a significant negative
correlation (from -0.3 to -0.5; $p < 0.001$) with rainfall during MAM and JJA and a significant positive correlation with
temperature during JJA (0.3; $p < 0.001$), which we do not currently understand. Fire emissions did not increase much where
we report the largest increases in methane emissions in 2020 or 2021, except over central Canadian provinces. (Figure A4).

185 To explore the robustness of our results, we explore a range sensitivity runs. First, we ran our inversion for 2020 with OH
concentrations decreased by 5% over regions with large anthropogenic emissions (as described in section 2.3), an estimate for
the value we expect based on widespread reductions in nitrogen oxide emissions due to shutting manufacturing and other

industries during Covid-19 lockdowns (Laughner et al. 2021). A reduction in OH, assuming constant emissions, would lead to an increase in atmospheric methane. Ignoring that possibility would result in a positive bias for reported methane emissions estimates. We find that our imposed 5% decrease in OH concentrations results in an emission reduction of 6.0 Tg/yr, representing 22% of the emission increase, relative to 2019, in the control run. Figure 4 show that the largest impacts of reducing OH on *a posteriori* methane emissions are of the order of $\pm 10\%$ over regions where there are the largest decreases in nitrogen oxide emissions (Cooper et al. 2022), including China, India, Europe, North America. The regions where values are higher than the control are a consequence of mass balance. Our 5% OH decrease cannot fully explain the increase in atmospheric methane, and consequently regions where OH were not decreased have had to compensate. The results for a smaller 1% decrease in OH have similar distributions but smaller changes (not shown). Second, we ran an experiment in which we used the methane columns determined by the proxy data, assuming model values for CO₂ (R. J. Parker et al. 2020). Using these data, we find our results for 2020 and 2021 are usually within a few percent of the values we report using the proxy data directly (Figure A6 and Figure A7). We found that assuming a different distribution for the OH reduction, based on observed changes in tropospheric ozone (Ziemke et al. 2022), did not significantly affect the results reported here (Appendix D). Including large, localized but short-term OH reductions also did not significantly impact our results. By including OH scaling factors into our state vector, we were able to infer simultaneously OH distributions and methane emissions (Appendix E). We find that the increased atmospheric growth rate of methane in 2020 that can be attributed to OH reductions is consistent with the values we reported from our experiments that used simpler *ad hoc* methods to describe reduced OH. Our *a posteriori* emission estimates from the control and the OH scaling inversions are consistent with independent observations from the TCCON network (Appendix C and E, respectively). Our sensitivity experiments provide confidence in our *a posteriori* emission estimates and in our statement that most of the atmospheric methane growth in 2020 was due to an increase in emissions, with the OH reduction associated with the Covid-19 lockdowns representing up to 30% of the global atmospheric methane growth.

210 **3 Concluding Remarks**

We reported regional emission estimates of methane during 2020 and 2021, two years with record-breaking atmospheric growth rates, inferred from satellite observations of methane from the Japanese Greenhouse gases Observing SATellite.

We find in both years that emissions from Eastern Africa, tropical Asia, and tropical South America dominate the global atmospheric growth rate, increasing by 11-13 Tg/yr, 4-8 Tg/yr, and 3-9 Tg relative to the 2019 baseline year, respectively. During 2020, we also find substantial increased emissions, relative to the 2019 baseline values, from Australia (3 ± 2 Tg) and temperate Eurasia (3 ± 5 Tg). Emission changes relative to 2019 are comparable in 2021, except for temperate South America that increases to 5 ± 3 Tg and temperate North America that increases to 3 ± 3 Tg. The elevated contributions we saw in 2020 over the western half of Africa (-5 ± 3 Tg) and Europe (-3 ± 3 Tg) are substantially reduced in 2021, compared to our 2019 baseline. We find statistically significant positive correlations between tropical methane emission and hydrological anomalies,

consistent with recent studies that have highlighted a growing role for microbial sources over the tropics (Lunt et al. 2019; Feng, Palmer, Zhu, et al. 2022; Wilson et al. 2020). Our results are broadly consistent with a recent study of the 2020 period (Qu et al. 2022), including the magnitude of change associated with a change in OH, albeit concluded using an independent method.

225

Substantial, widespread reductions in nitrogen oxides during 2020 associated with the shutdown of manufacturing and other industries will have perturbed atmospheric concentrations of the OH loss of methane. A reduction in OH could also help explain, in principle, the record-breaking atmospheric increase in methane. Here we explore that issue by scaling back our prescribed OH fields by 5% over fossil fuel combustion regions to assess the impact of our reported increases in methane emissions. We find a 5% decrease in OH results in an *a posteriori* emission reduction of 6.0 Tg compared to our control run that does not consider a decrease in OH, equivalent to 22% of the emission increase in our control run for 2020. These changes are mainly focused over fossil fuel emitting regions, as expected. Other sensitivity experiments that explored alternative distributions of OH reductions and an inversion that included OH scaling factors found similar results, with OH reductions explaining up to 30% of the global atmospheric methane growth rate in 2020. Our results suggest that an increase in emissions was predominately responsible for the observed growth in atmospheric methane during 2020.

230

235

This study highlights the tremendous value of using satellite observations to understand rapid changes in atmospheric methane. They provide crucial information not only to identify regional column hotspots associated with emissions but also provide correlative information to help attribute those hotspots to specific anthropogenic or natural emissions.

240

Data availability. The University of Leicester GOSAT Proxy v9.0 XCH₄ data are available from the Centre for Environmental Data Analysis data repository at <https://doi.org/10.5285/18ef8247f52a4cb6a14013f8235cc1eb>. Precipitation, temperature, and the GRACE datasets are available at <http://grace.jpl.nasa.gov>. The community-led GEOS-Chem model of atmospheric chemistry and model is maintained centrally by Harvard University (<http://geos-chem.seas.harvard.edu>), and is available on request. The ensemble Kalman filter code is publicly available as PyOSSE (<https://www.nceo.ac.uk/data-tools/atmospheric-tools/>). The TCCON data were obtained from the TCCON Data Archive hosted by CaltechDATA at <https://tccodata.org>.

245

Author contributions. LF and PIP designed the research; LF and MFL prepared the calculations; RJP and HB provided the GOSAT data and expert advice on its usage; PIP wrote the paper, with comments from LF, RJP, MFL, and HB.

250

Competing interests. The contact author has declared that neither they nor their co-authors have any competing interests.

Acknowledgements: We thank the Japanese Aerospace Exploration Agency, National Institute for Environmental Studies, and the Ministry of Environment for the GOSAT data and their continued support as part of the Joint Research Agreements at the Universities of Edinburgh and Leicester. GOSAT retrievals were processed using the ALICE High-Performance Computing Facility at the University of Leicester. We thank all the scientists that submitted data to the CO₂ and methane Observation Package (ObsPack) data products, coordinated by NOAA ESRL, and making them freely available for carbon cycle research. We also thank the GEOS-Chem community, particularly the team at Harvard University who help maintain the GEOS-Chem model, and the NASA Global Modeling and Assimilation Office (GMAO) who provide the MERRA2 data product.

260

Financial support: L.F., P.I.P., R.J.P., and H.B. acknowledge support from the UK National Centre for Earth Observation funded by the National Environment Research Council (NE/R016518/1); R.J.P. also acknowledges funding from grant NE/N018079/1. We acknowledge funding from the Copernicus Climate Change Service (C3S2_312a_Lot2) related to generation of the GOSAT data.

265 **References**

- Bloom, A A, K W Bowman, M Lee, A J Turner, R Schroeder, J R Worden, R Weidner, K C McDonald, and D J Jacob. 2017. “A Global Wetland Methane Emissions and Uncertainty Dataset for Atmospheric Chemical Transport Models (WetCHARTs Version 1.0).” *Geoscientific Model Development* 10 (6): 2141–56. <https://doi.org/10.5194/gmd-10-2141-2017>.
- 270 Bosilovich, M. G, S Akella, L Coy, R Cullather, C Draper, R Gelaro, R Kovach, et al. 2015. “MERRA-2: Initial Evaluation of the Climate.”
- Buschmann, M, C Petri, M Palm, T Warneke, and J Notholt. 2022. “TCCON Data from Ny-Ålesund, Svalbard (NO), Release GGG2020.R0.” CaltechDATA. <https://doi.org/10.14291/tcon.ggg2020.nyalesund01.R0>.
- Ciavarella, Andrew, Daniel Cotterill, Peter Stott, Sarah Kew, Sjoukje Philip, Geert Jan van Oldenborgh, Amalie Skålevåg, et al. 2021. “Prolonged Siberian Heat of 2020 Almost Impossible without Human Influence.” *Climatic Change* 166 (1): 9.
- 275 Cooper, Matthew J., Randall V. Martin, Melanie S. Hammer, Pieternel F. Levelt, Pepijn Veeffkind, Lok N. Lamsal, Nikolay A. Krotkov, Jeffrey R. Brook, and Chris A. McLinden. 2022. “Global Fine-Scale Changes in Ambient NO₂ during COVID-19 Lockdowns.” *Nature* 601 (7893). <https://doi.org/10.1038/s41586-021-04229-0>.
- Cox, Adam, Alcide Giorgio Di Sarra, Anna Karion, Arlyn Andrews, Aurelie Colomb, Bert Scheeren, Bill Paplawsky, et al. 280 2022. “Multi-Laboratory Compilation of Atmospheric Carbon Dioxide Data for the Year 2021; Obspack_co2_1_NRT_v7.1_2022-03-04.” NOAA Earth System Research Laboratory, Global Monitoring Laboratory. <https://doi.org/10.25925/20220301>.
- Cox, Adam, Alcide Giorgio Di Sarra, Alex Vermeulen, Alistair Manning, Andreas Beyersdorf, Andreas Zahn, Andrew Manning, et al. 2021. “Multi-Laboratory Compilation of Atmospheric Carbon Dioxide Data for the Period 1957-2020;

- 285 Obspack_co2_1_GLOBALVIEWplus_v7.0_2021-08-18.” NOAA Global Monitoring Laboratory.
<https://doi.org/10.25925/20210801>.
- Etiopie, E. 2015. *Natural Gas Seepage: The Earth’s Hydrocarbon Degassing*. Springer.
- Feng, L., Paul I Palmer, Hartmut Bösch, Robert J Parker, Alex J Webb, Caio S C Correia, Nicholas M Deutscher, et al. 2017.
“Consistent Regional Fluxes of CH₄ and CO₂ Inferred from GOSAT Proxy XCH₄: XCO₂ Retrievals, 2010–2014.”
290 *Atmos. Chem. Phys* 17: 4781–97.
- Feng, L., Paul I Palmer, Sihong Zhu, Robert J Parker, and Yi Liu. 2022. “Tropical Methane Emissions Explain Large Fraction
of Recent Changes in Global Atmospheric Methane Growth Rate.” *Nature Communications* 13 (1): 1378.
<https://doi.org/10.1038/s41467-022-28989-z>.
- Feng, L, P I Palmer, R J Parker, M F Lunt, and H Boesch. 2022. “Methane Emissions Responsible for Record-Breaking
295 Atmospheric Methane Growth Rates in 2020 and 2021.” *Atmos. Chem. Phys. Discuss.* 2022 (June): 1–23.
<https://doi.org/10.5194/acp-2022-425>.
- Fraser, A., P. I. Palmer, L. Feng, H. Bösch, R. Parker, E. J. Dlugokencky, P. B. Krummel, and R. L. Langenfelds. 2014a.
“Estimating Regional Fluxes of CO₂ and CH₄ Using Space-Borne Observations of XCH₄: XCO₂.” *Atmospheric
Chemistry and Physics* 14 (23). <https://doi.org/10.5194/acp-14-12883-2014>.
- 300 Fraser, A, P I Palmer, L Feng, H Bösch, R Parker, E J Dlugokencky, P B Krummel, and R L Langenfelds. 2014b. “Estimating
Regional Fluxes of CO₂ and CH₄ Using Space-Borne Observations of XCH₄: XCO₂.” *Atmospheric Chemistry and
Physics* 14 (23): 12883–95. <https://doi.org/10.5194/acp-14-12883-2014>[FL1].
- Fung, I, J John, J Lerner, E Matthews, M Prather, L P Steele, and P J Fraser. 1991. “Three-Dimensional Model Synthesis of
the Global Methane Cycle.” *Journal of Geophysical Research: Atmospheres* 96 (D7): 13033–65.
305 <https://doi.org/https://doi.org/10.1029/91JD01247>.
- García, O E, M Schneider, B Herkommer, J Gross, F Hase, T Blumenstock, and E Sepúlveda. 2022. “TCCON Data from Izana
(ES), Release GGG2020.R1.” CaltechDATA. <https://doi.org/10.14291/tcon.ggg2020.izana01.R1>.
- Gurney, Kevin Robert, Rachel M Law, A Scott Denning, Peter J Rayner, Bernard C Pak, David Baker, Philippe Bousquet, et
al. 2004. “Transcom 3 Inversion Intercomparison: Model Mean Results for the Estimation of Seasonal Carbon Sources
310 and Sinks.” *Global Biogeochemical Cycles* 18 (1).
- Hase, F, B Herkommer, J Groß, T Blumenstock, M.ä. Kiel, and S Dohe. 2022. “TCCON Data from Karlsruhe (DE), Release
GGG2020.R0.” CaltechDATA. <https://doi.org/10.14291/tcon.ggg2020.karlsruhe01.R0>.
- Janssens-Maenhout, G, M Crippa, D Guizzardi, M Muntean, E Schaaf, F Dentener, P Bergamaschi, et al. 2019. “EDGAR
v4.3.2 Global Atlas of the Three Major Greenhouse Gas Emissions for the Period 1970–2012.” *Earth System Science
Data* 11 (3): 959–1002. <https://doi.org/10.5194/essd-11-959-2019>.
- 315 Kivi, R, P Heikkinen, and E Kyrö. 2022. “TCCON Data from Sodankylä (FI), Release GGG2020.R0.” CaltechDATA.
<https://doi.org/10.14291/tcon.ggg2020.sodankyla01.R0>.
- Kvenvolden, K A, and B W Rogers. 2005. “Gaia’s Breath’s Global Methane Exhalations.” *Marine and Petroleum Geology* 22

(4): 579–90. <https://doi.org/https://doi.org/10.1016/j.marpetgeo.2004.08.004>.

- 320 Landerer, Felix W, Frank M Flechtner, Himanshu Save, Frank H Webb, Tamara Bandikova, William I Bertiger, Srinivas V Bettadpur, et al. 2020. “Extending the Global Mass Change Data Record: {GRACE} Follow-On Instrument and Science Data Performance.” *Geophysical Research Letters* 47 (12). <https://doi.org/10.1029/2020gl088306>.
- Laughner, Joshua L., Jessica L. Neu, David Schimel, Paul O. Wennberg, Kelley Barsanti, Kevin W. Bowman, Abhishek Chatterjee, et al. 2021. “Societal Shifts Due to COVID-19 Reveal Large-Scale Complexities and Feedbacks between
325 Atmospheric Chemistry and Climate Change.” *Proceedings of the National Academy of Sciences of the United States of America* 118 (46). <https://doi.org/10.1073/pnas.2109481118>.
- Liu, Cheng, Wei Wang, Youwen Sun, and Changgong Shan. 2022. “TCCON Data from Hefei (PRC), Release GGG2020.R0.” CaltechDATA. <https://doi.org/10.14291/tccon.ggg2020.hefei01.R0>.
- Lunt, M. F., P I Palmer, L Feng, C M Taylor, H Boesch, and R J Parker. 2019. “An Increase in Methane Emissions from
330 Tropical Africa between 2010 and 2016 Inferred from Satellite Data.” *Atmos. Chem. Phys.* 19 (23): 14721–40. <https://doi.org/10.5194/acp-19-14721-2019>.
- Lunt, M F, P I Palmer, A Lorente, T Borsdorff, J Landgraf, R J Parker, and H Boesch. 2021. “Rain-Fed Pulses of Methane from East Africa during 2018-2019 Contributed to Atmospheric Growth Rate.” *Environmental Research Letters* 16 (2): 24021. <https://doi.org/10.1088/1748-9326/abd8fa>.
- 335 Mao, Jingqiu, Fabien Paulot, Daniel J Jacob, Ronald C Cohen, John D Crouse, Paul O Wennberg, Christoph A Keller, Rynda C Hudman, Michael P Barkley, and Larry W Horowitz. 2013. “Ozone and Organic Nitrates over the Eastern United States: Sensitivity to Isoprene Chemistry.” *Journal of Geophysical Research: Atmospheres* 118 (19): 11,211–256,268. <https://doi.org/https://doi.org/10.1002/jgrd.50817>.
- Mazière, M De, M K Sha, F Desmet, C Hermans, F Scolas, N Kumps, M Zhou, J.-M. Metzger, V Dufлот, and J.-P. Cammas.
340 2022. “TCCON Data from Réunion Island (RE), Release GGG2020.R0.” CaltechDATA. <https://doi.org/10.14291/tccon.ggg2020.reunion01.R0>.
- McNorton, J, N Bousserez, A Agustí-Panareda, G Balsamo, L Cantarello, R Engelen, V Huijnen, et al. 2022. “Quantification of Methane Emissions from Hotspots and during COVID-19 Using a Global Atmospheric Inversion.” *Atmos. Chem. Phys.* 22 (9): 5961–81. <https://doi.org/10.5194/acp-22-5961-2022>.
- 345 Miyazaki, Kazuyuki, Kevin Bowman, Takashi Sekiya, Masayuki Takigawa, Jessica L. Neu, Kengo Sudo, Greg Osterman, and Henk Eskes. 2021. “Global Tropospheric Ozone Responses to Reduced NO_x Emissions Linked to the COVID-19 Worldwide Lockdowns.” *Science Advances* 7 (24). <https://doi.org/10.1126/sciadv.abf7460>.
- Morino, I., Voltaire A Velazco, Akihiro Hori, Osamu Uchino, and David W T Griffith. 2022. “TCCON Data from Burgos, Ilocos Norte (PH), Release GGG2020.R0.” CaltechDATA. <https://doi.org/10.14291/tccon.ggg2020.burgos01.R0>.
- 350 Morino, I, H Ohyama, A Hori, and H Ikegami. 2022a. “TCCON Data from Rikubetsu (JP), Release GGG2020.R0.” CaltechDATA. <https://doi.org/10.14291/tccon.ggg2020.rikubetsu01.R0>.
- . 2022b. “TCCON Data from Tsukuba (JP), 125HR, Release GGG2020.R0.” CaltechDATA.

<https://doi.org/10.14291/tccon.ggg2020.tsukuba02.R0>.

- 355 Notholt, J, C Petri, T Warneke, and M Buschmann. 2022. “TCCON Data from Bremen (DE), Release GGG2020.R0.” CaltechDATA. <https://doi.org/10.14291/tccon.ggg2020.bremen01.R0>.
- Oda, T, and S Maksyutov. 2021. “ODIAC Fossil Fuel CO₂ Emissions Dataset (Version Name: ODIAC2020b).” Center for Global Environmental Research, National Institute for Environmental Studies. <https://doi.org/10.17595/20170411.001>.
- 360 Palmer, P I, L Feng, M F Lunt, R J Parker, H Bösch, X Lan, L Alba, and B Tobiaa. 2021. “The Added Value of Satellite Observations of Methane for Understanding the Contemporary Methane Budget.” *Phil. Trans. R. Soc. A* 379 (20210106). <https://doi.org/http://doi.org/10.1098/rsta.2021.0106>.
- Pandey, Sudhanshu, Sander Houweling, Maarten Krol, Ilse Aben, Guillaume Monteil, Narcisa Nechita-Banda, Edward J Dlugokencky, et al. 2017. “Enhanced Methane Emissions from Tropical Wetlands during the 2011 La Niña.” *Scientific Reports* 7 (1). <https://doi.org/10.1038/srep45759>.
- 365 Pandey, Sudhanshu, Sander Houweling, Alba Lorente, Tobias Borsdorff, Maria Tsvilidou, A. Anthony Bloom, Benjamin Poulter, Zhen Zhang, and Ilse Aben. 2021. “Using Satellite Data to Identify the Methane Emission Controls of South Sudan’s Wetlands.” *Biogeosciences*. <https://doi.org/10.5194/bg-18-557-2021>.
- Parker, R., and Hartmut Boesch. 2020. “University of Leicester GOSAT Proxy XCH₄ v9.0.” Centre for Environmental Data Analysis.
- Parker, R J, Alex Webb, Hartmut Boesch, Peter Somkuti, Rocio Barrio Guillo, Antonio Di Noia, Nikoleta Kalaitzi, et al. 2020. 370 “A Decade of GOSAT Proxy Satellite CH₄ Observations.” *Earth System Science Data* 12 (4). <https://doi.org/10.5194/essd-12-3383-2020>.
- Petri, Christof, Mihalis Vrekoussis, Constantina Rousogenous, Thorsten Warneke, Jean Sciare, and Justus Notholt. 2022. “TCCON Data from Nicosia (CY), Release GGG2020.R0.” CaltechDATA. <https://doi.org/10.14291/tccon.ggg2020.nicosia01.R0>.
- 375 Pollard, David Frank, John Robinson, and Hisako Shiona. 2022. “TCCON Data from Lauder (NZ), Release GGG2020.R0.” CaltechDATA. <https://doi.org/10.14291/tccon.ggg2020.lauder03.R0>.
- Qu, Zhen, Daniel J Jacob, Yuzhong Zhang, Lu Shen, Daniel J Varon, Xiao Lu, Tia Scarpelli, Anthony Bloom, John Worden, and Robert J Parker. 2022. “Attribution of the 2020 Surge in Atmospheric Methane by Inverse Analysis of GOSAT Observations.” *Environmental Research Letters* 17 (9): 094003. <https://doi.org/10.1088/1748-9326/ac8754>.
- 380 Randerson, James T., Matthew V. Thompson, Carolyn M. Malmstrom, Christopher B. Field, and Inez Y. Fung. 1996. “Substrate Limitations for Heterotrophs: Implications for Models That Estimate the Seasonal Cycle of Atmospheric CO₂.” *Global Biogeochemical Cycles* 10 (4). <https://doi.org/10.1029/96GB01981>.
- Rigby, M, R G Prinn, P J Fraser, P G Simmonds, R L Langenfelds, J Huang, D M Cunnold, et al. 2008. “Renewed Growth of Atmospheric Methane.” *Geophysical Research Letters* 35 (22). <https://doi.org/https://doi.org/10.1029/2008GL036037>.
- 385 Sarra, Alcide Giorgio Di, Ankur Desai, Anna Karion, Arlyn Andrews, Aurelie Colomb, Bert Scheeren, Brian Viner, et al. 2022. “Multi-Laboratory Compilation of Atmospheric Methane Data for the Year 2021;

- Obspack_ch4_1_NRT_v4.0_2022-03-03.” NOAA Earth System Research Laboratory, Global Monitoring Laboratory.
<https://doi.org/10.25925/20211101>.
- 390 Sarra, Alcide Giorgio Di, Andreas Zahn, Andrew Watson, Ankur Desai, Anna Karion, Arlyn Andrews, Aurelie Colomb, et al.
2021. “Multi-Laboratory Compilation of Atmospheric Methane Data for the Period 1983–2020;
Obspack_ch4_1_GLOBALVIEWplus_v4.0_2021-10-14.” NOAA Global Monitoring Laboratory.
<https://doi.org/10.25925/20211001>.
- Shiomi, K, S Kawakami, H Ohyama, K Arai, H Okumura, H Ikegami, and M Usami. 2022. “TCCON Data from Saga (JP),
Release GGG2020.R0.” CaltechDATA. <https://doi.org/10.14291/tccon.ggg2020.saga01.R0>.
- 395 Takahashi, Taro, Stewart C Sutherland, Rik Wanninkhof, Colm Sweeney, Richard A Feely, David W Chipman, Burke Hales,
et al. 2009. “Climatological Mean and Decadal Change in Surface Ocean PCO₂, and Net Sea-Air CO₂ Flux over the
Global Oceans.” *Deep Sea Research Part II: Topical Studies in Oceanography* 56 (8): 554–77.
<https://doi.org/https://doi.org/10.1016/j.dsr2.2008.12.009>.
- Té, Y, P Jeseck, and C Janssen. 2022. “TCCON Data from Paris (FR), Release GGG2020.R0.” CaltechDATA.
400 <https://doi.org/10.14291/tccon.ggg2020.paris01.R0>.
- Thanwerdas, J, M Saunois, A Berchet, I Pison, D Hauglustaine, M Ramonet, C Crevoisier, B Baier, C Sweeney, and P
Bousquet. 2019. “Impact of Atomic Chlorine on the Modelling of Total Methane and Its ¹³C:¹²C Isotopic Ratio at Global
Scale.” *Atmospheric Chemistry and Physics Discussions* 2019: 1–28. <https://doi.org/10.5194/acp-2019-925>.
- Turner, A J, D J Jacob, K J Wecht, J D Maasackers, E Lundgren, A E Andrews, S C Biraud, et al. 2015. “Estimating Global
405 and North American Methane Emissions with High Spatial Resolution Using GOSAT Satellite Data.” *Atmospheric
Chemistry and Physics* 15 (12): 7049–69. <https://doi.org/10.5194/acp-15-7049-2015>.
- Warneke, T, C Petri, J Notholt, and M Buschmann. 2022. “TCCON Data from Orléans (FR), Release GGG2020.R0.”
CaltechDATA. <https://doi.org/10.14291/tccon.ggg2020.orleans01.R0>.
- Wennberg, P O, C M Roehl, D Wunch, J.-F. Blavier, G C Toon, N T Allen, R Treffers, and J Laughner. 2022. “TCCON Data
410 from Caltech (US), Release GGG2020.R0.” CaltechDATA. <https://doi.org/10.14291/tccon.ggg2020.pasadena01.R0>.
- Wennberg, P O, C M Roehl, D Wunch, G C Toon, J.-F. Blavier, R Washenfelder, G Keppel-Aleks, and N T Allen. 2022.
“TCCON Data from Park Falls (US), Release GGG2020.R0.” CaltechDATA.
<https://doi.org/10.14291/tccon.ggg2020.parkfalls01.R0>.
- Wennberg, P O, D Wunch, C M Roehl, J.-F. Blavier, G C Toon, and N T Allen. 2022. “TCCON Data from Lamont (US),
415 Release GGG2020.R0.” CaltechDATA. <https://doi.org/10.14291/tccon.ggg2020.lamont01.R0>.
- Werf, G R van der, J T Randerson, L Giglio, T T van Leeuwen, Y Chen, B M Rogers, M Mu, et al. 2017. “Global Fire
Emissions Estimates during 1997–2016.” *Earth System Science Data* 9 (2): 697–720. <https://doi.org/10.5194/essd-9-697-2017>.
- Wilson, C, M P Chipperfield, M Gloor, R J Parker, H Boesch, J McNorton, L V Gatti, J B Miller, L S Basso, and S A Monks.
420 2020. “Large and Increasing Methane Emissions from Eastern Amazonia Derived from Satellite Data, 2010–2018.”

Atmospheric Chemistry and Physics Discussions 2020: 1–38. <https://doi.org/10.5194/acp-2020-1136>.

Wunch, D, J Mendonca, O Colebatch, N T Allen, J.-F. Blavier, K Kunz, S Roche, et al. 2022. “TCCON Data from East Trout Lake, SK (CA), Release GGG2020.R0.” CaltechDATA. <https://doi.org/10.14291/tccon.ggg2020.easttroutlake01.R0>.

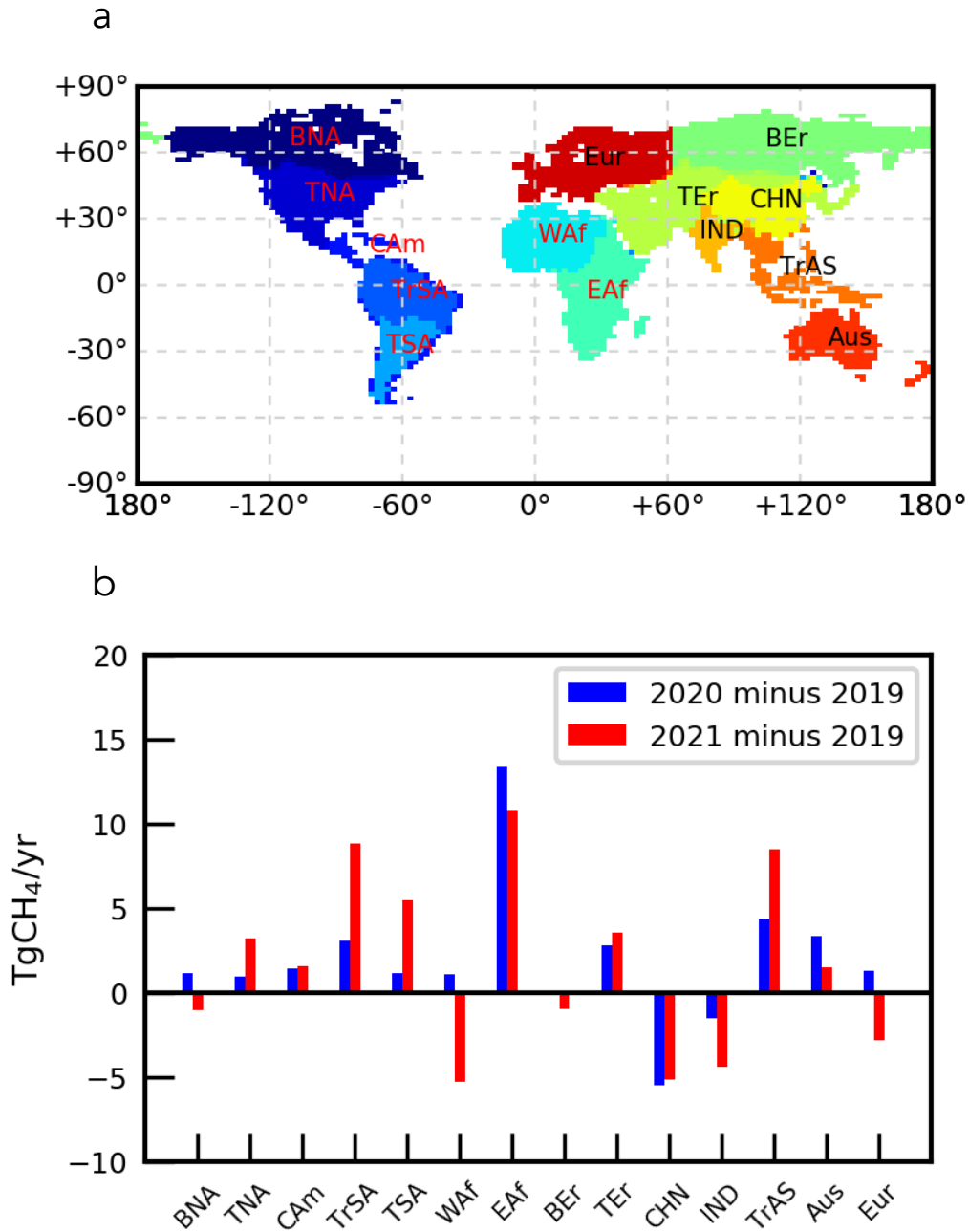
425 Xie, P, and P A Arkin. 1997. “Global Precipitation: A 17-Year Monthly Analysis Based on Gauge Observations, Satellite Estimates, and Numerical Model Outputs.” *Bulletin of the American Meteorological Society* 78 (11): 2539–58. [https://doi.org/10.1175/1520-0477\(1997\)078<2539:GPAYMA>2.0.CO;2](https://doi.org/10.1175/1520-0477(1997)078<2539:GPAYMA>2.0.CO;2).

Zhou, Minqiang, Pucai Wang, Nicolas Kumps, Christian Hermans, and Weidong Nan. 2022. “TCCON Data from Xianghe, China, Release GGG2020.R0.” CaltechDATA. <https://doi.org/10.14291/tccon.ggg2020.xianghe01.R0>.

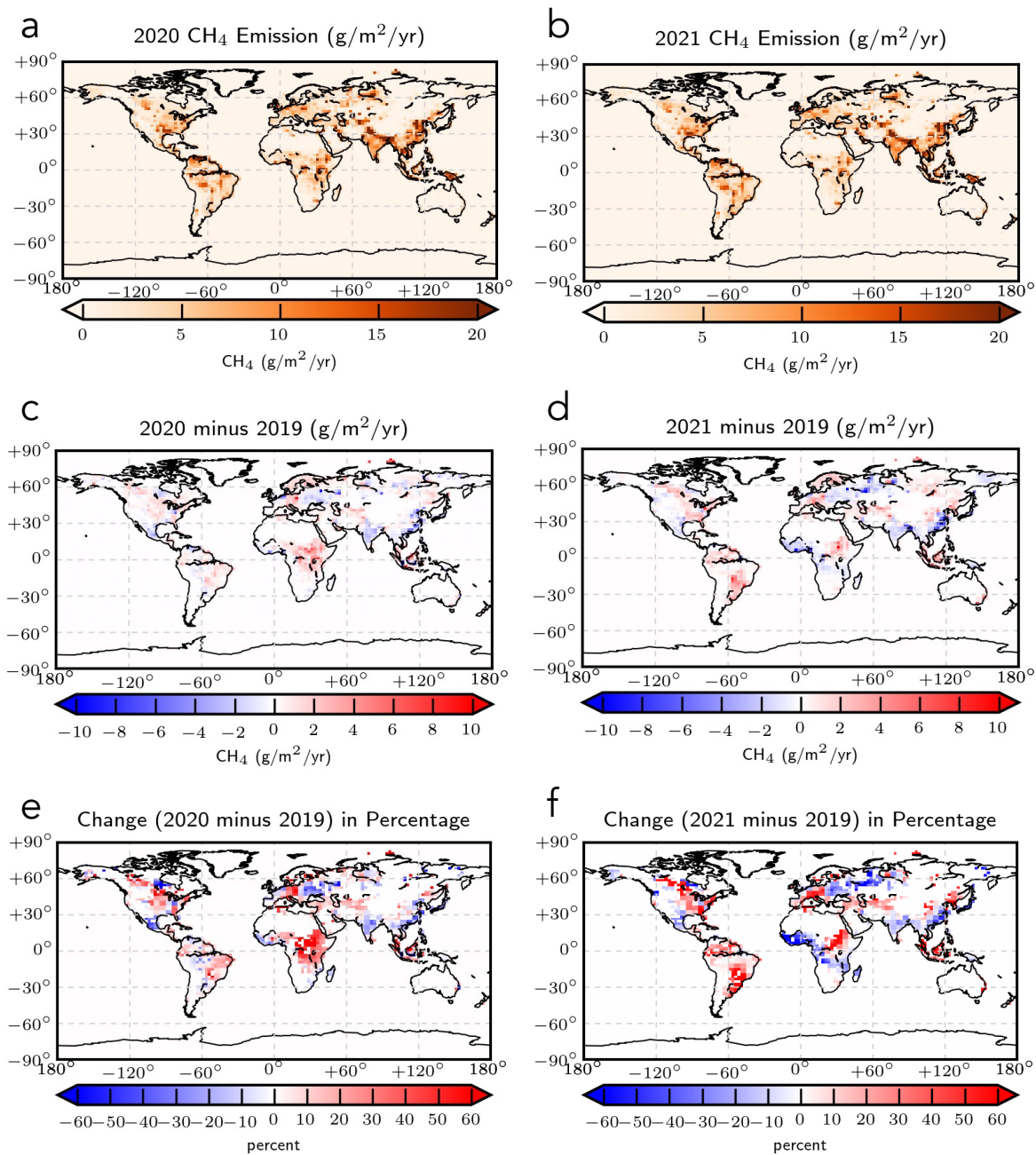
430 Ziemke, Jerry R, Natalya A Kramarova, Stacey M Frith, Liang-Kang Huang, David P Haffner, Krzysztof Wargan, Lok N Lamsal, Gordon J Labow, Richard D McPeters, and Pawan K Bhartia. 2022. “NASA Satellite Measurements Show Global-Scale Reductions in Free Tropospheric Ozone in 2020 and Again in 2021 During COVID-19.” *Geophysical Research Letters* 49 (15): e2022GL098712. <https://doi.org/https://doi.org/10.1029/2022GL098712>.

435

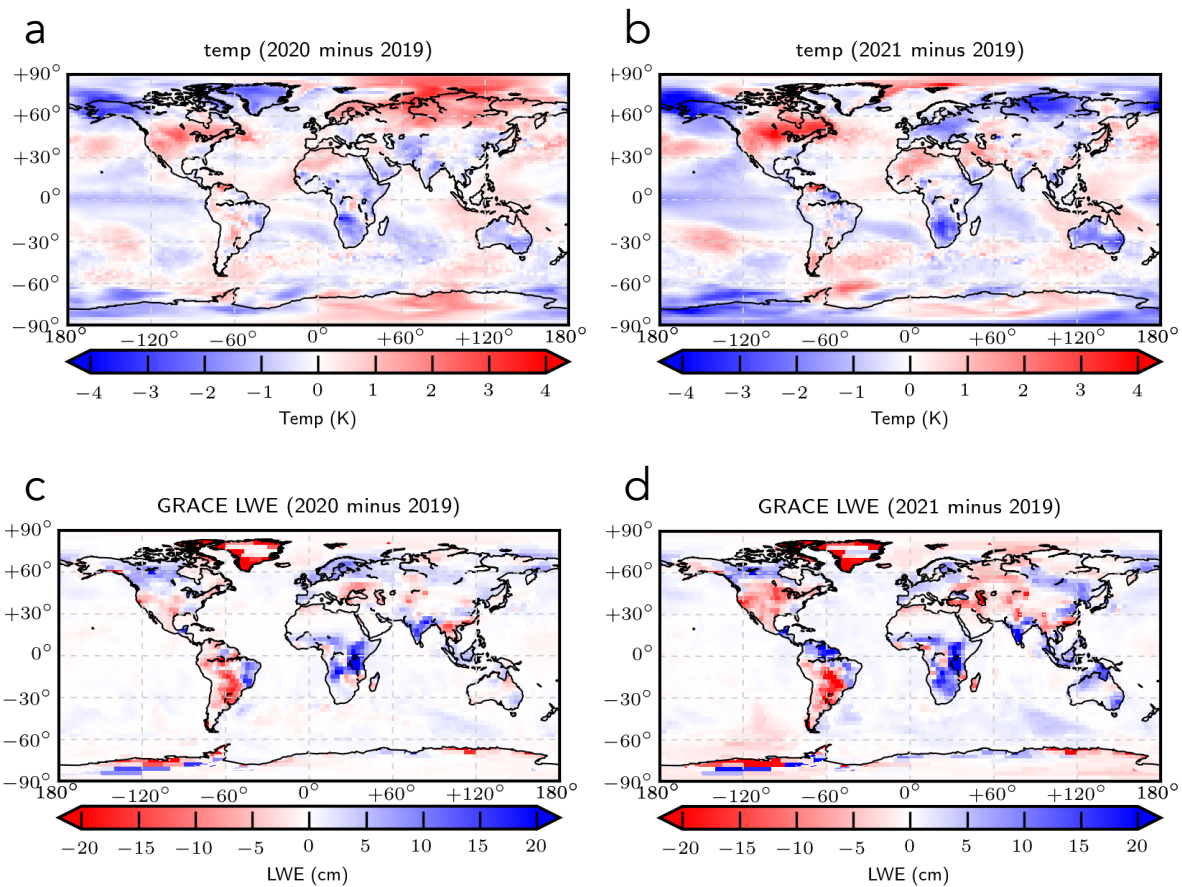
Figures



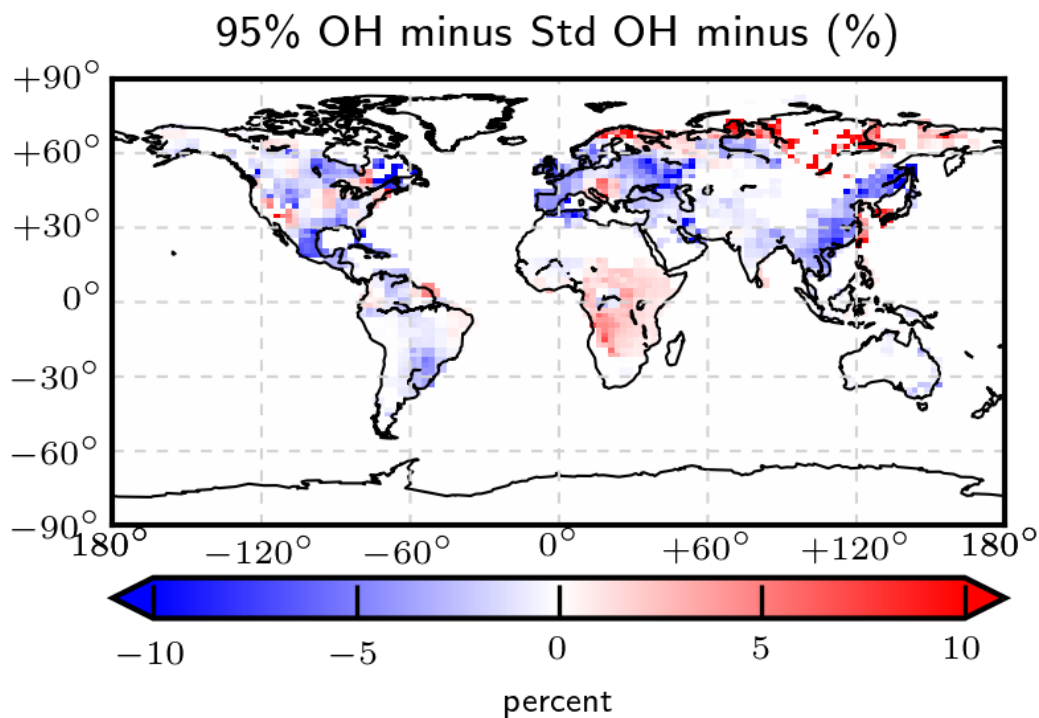
440 **Figure 1** Large-scale geographical regions a) for which we report methane changes (TgCH₄/yr) in 2020 and 2021 b) relative to our 2019 baseline year. Geographical regions, informed by TransCom-3 experiments (Gurney et al. 2004), include boreal North America (BNA), temperate North America (TNA), central America (Cam), tropical South America (TrSA), temperate South America (TSA), Europe (Eur), western Africa (Waf), eastern Africa (Eaf), boreal Eurasia (BEr), temperate Eurasia (TEr), India (IND), China (CHN), tropical Asia (TrAs), and Australia (Aus).



445 **Figure 2** Global *a posteriori* emissions of methane (g/m²/yr) inferred from GOSAT methane:CO₂ column ratio data for 2020 (panel a) and 2021 (panel b) and how they differ from the baseline year of 2019, described in terms of absolute (panels c and d, respectively) and percentage values (panels e and f).



450 **Figure 3** Global annual mean surface temperature and GRACE liquid water equivalent (LWE) anomalies in 2020 (panel a and c) and 2021 (panels b and d) relative to values in 2019.



455 **Figure 4** Percentage difference in global *a posteriori* methane emissions inferred from GOSAT for 2020 between a sensitivity run in which the OH field was decreased by 5% and the control run (Figure 2).

Tables

| | Global annual methane emissions (Tg/yr) | | |
|---------------------------------------|---|------------|------------|
| | 2019 | 2020 | 2021 |
| GOSAT | 583.7±11.2 | 610.7±11.3 | 609.5±12.0 |
| GOSAT with OH decreased by 5% | | 604.7±11.3 | |
| <i>In situ</i> | 588.9±18.1 | 601.4±18.6 | -- |
| | | | |
| NOAA atmospheric growth rate (ppb/yr) | 9.89±0.64 | 15.29±0.38 | 16.94±0.38 |

Table 1 Global annual emission estimates of methane (Tg/yr) inferred from GOSAT (2019-2021) and *in situ* (2019-2020) atmospheric measurements of methane. The annual atmospheric methane growth rate (ppb/yr) for 2019 to 2022 reported by NOAA is also shown.

Appendix A: supplementary figures

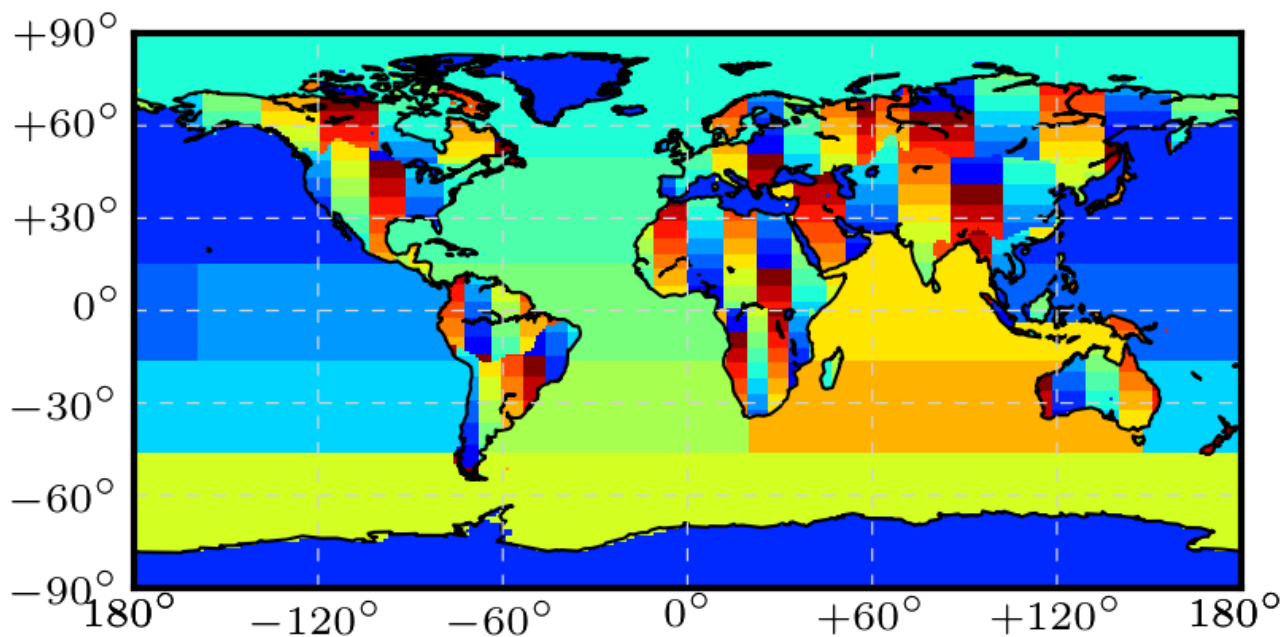


Figure A1 Basis functions that describe the 487 regions where we estimate methane emissions, including 476 land regions and 11 oceanic regions.

465

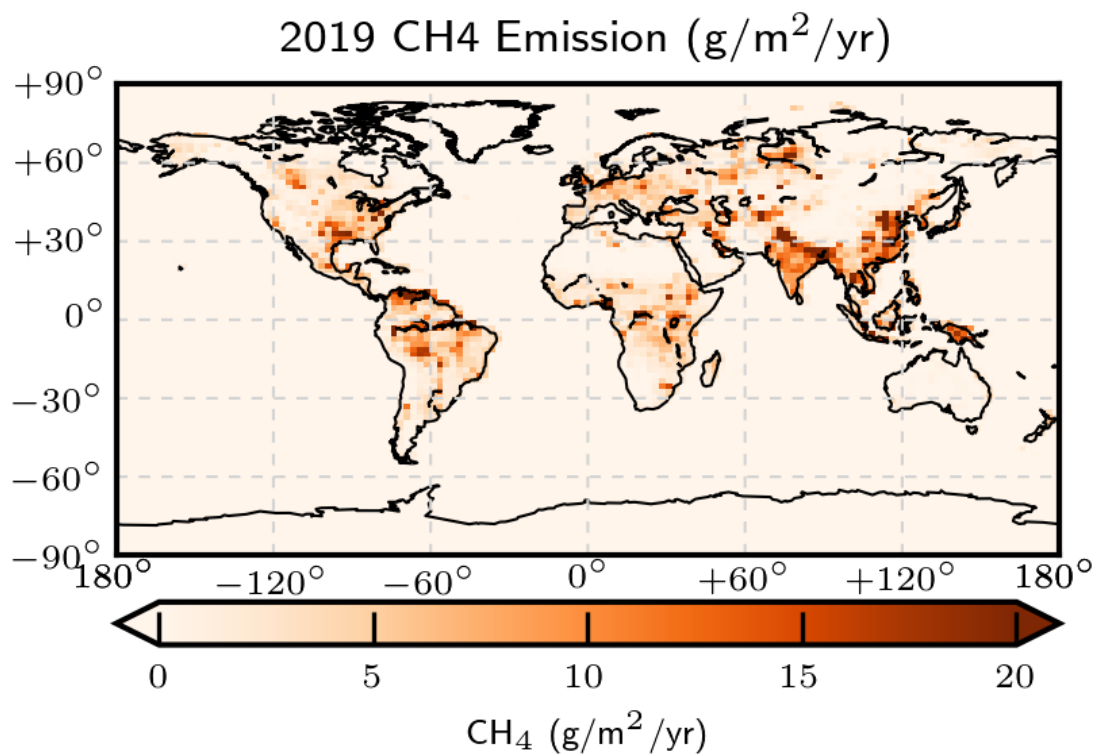
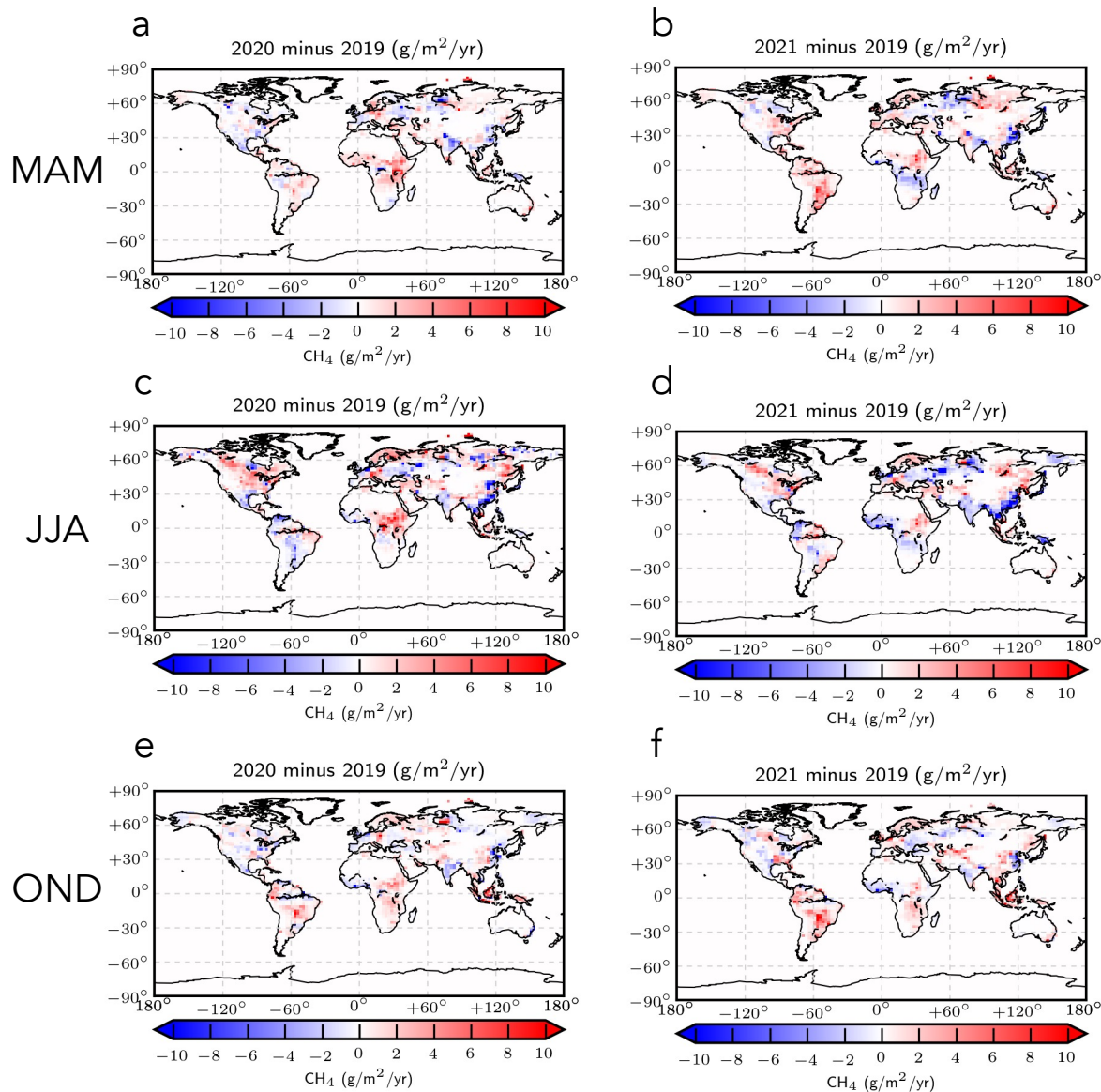
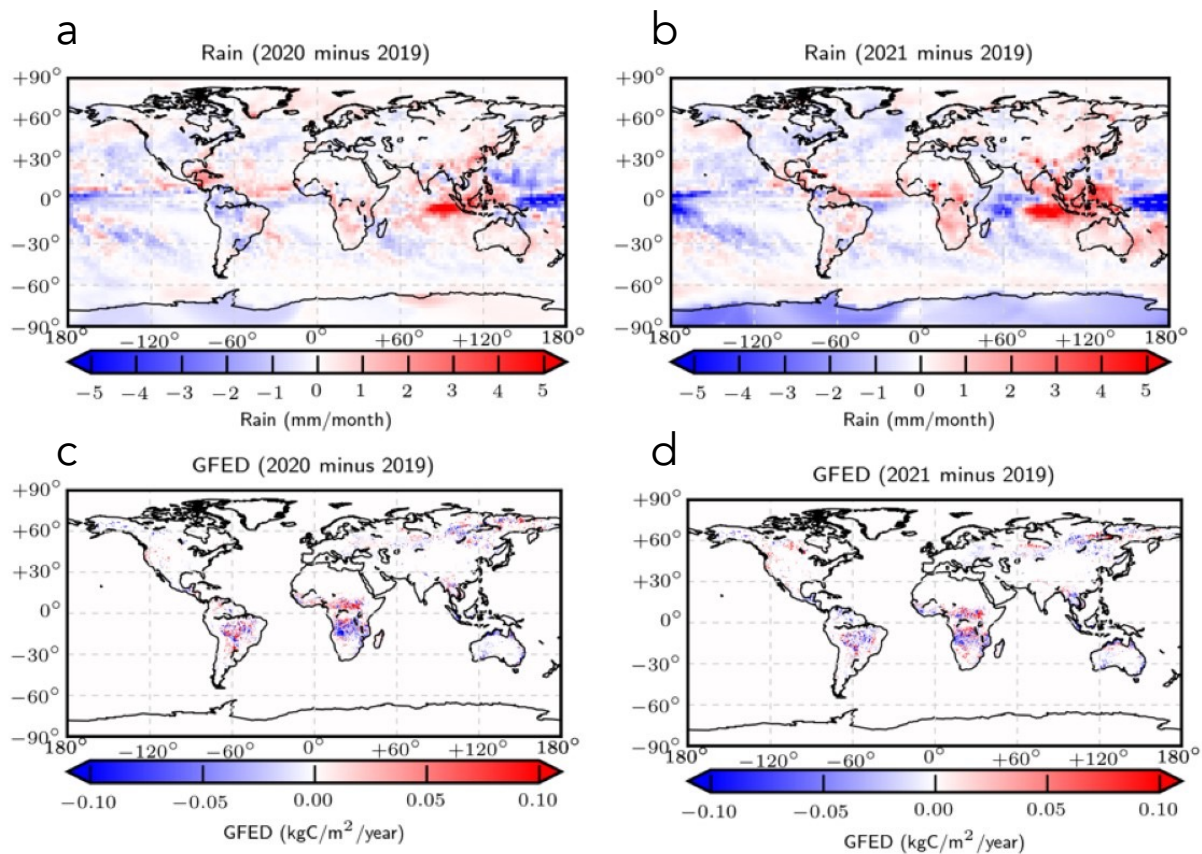


Figure A2 Global *a posteriori* emissions of methane (g/m²/yr) inferred from GOSAT methane:CO₂ column ratio data for the baseline year of 2019 (Feng, Palmer, Zhu, et al. 2022).



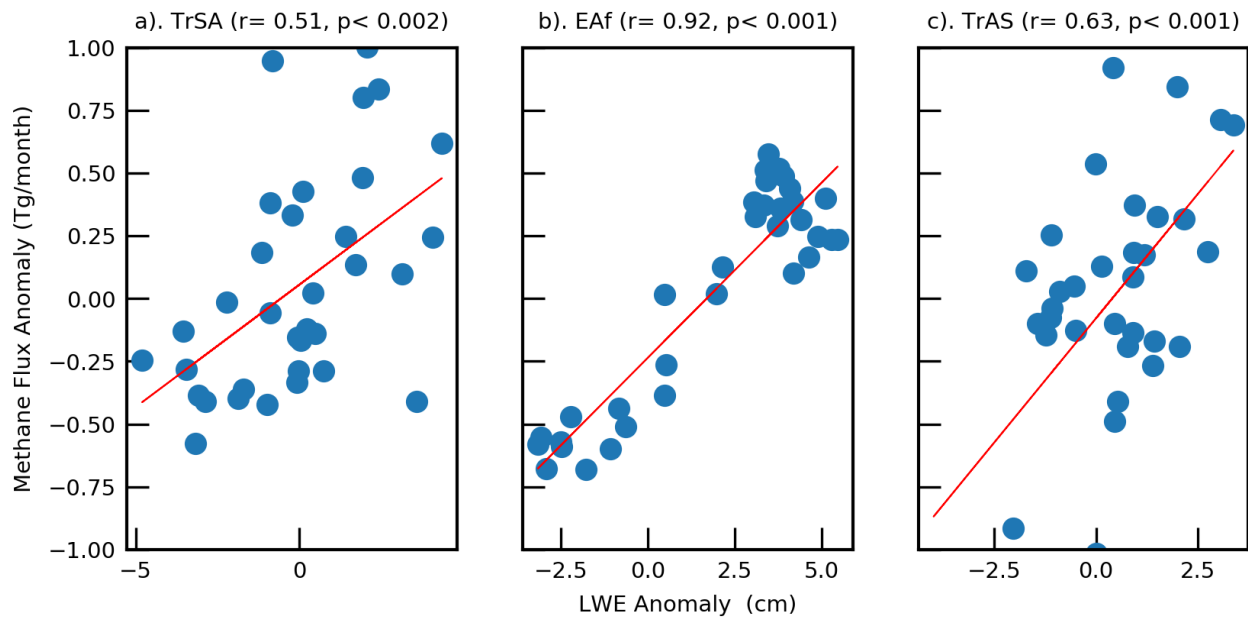
470

Figure A3 Global seasonal *a posteriori* emissions of methane ($\text{g/m}^2/\text{yr}$) inferred from GOSAT methane: CO_2 column ratio data for 2020 (l.h.s. panels) and 2021 (r.h.s. panels) relative to the baseline year of 2019, described in terms of absolute values. Seasons are based on rainfall changes over the tropics.

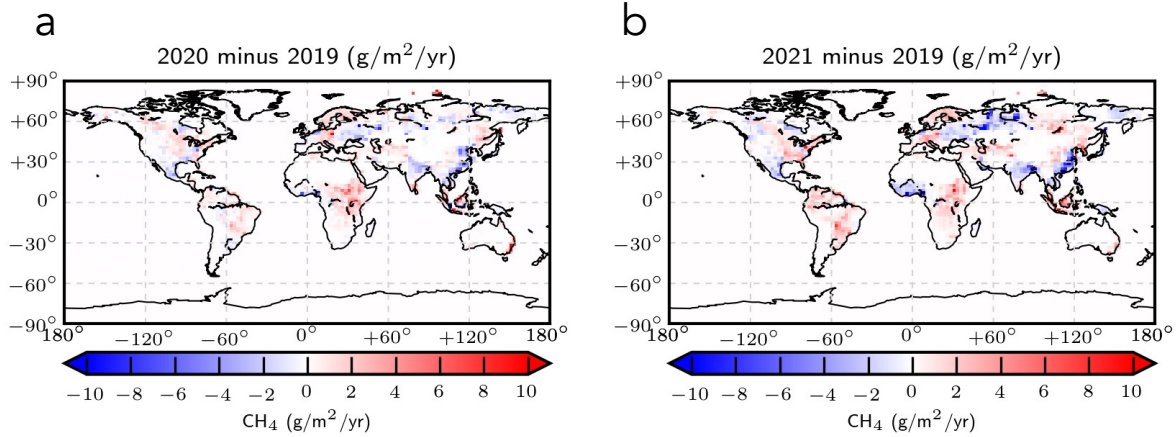


475

Figure A4 Global annual mean NOAA CMAP precipitation (mm/month/yr) and GFED fire emission (kgC/m²/yr) anomalies in 2020 (panel a and c) and 2021 (panels b and d) relative to values in 2019.

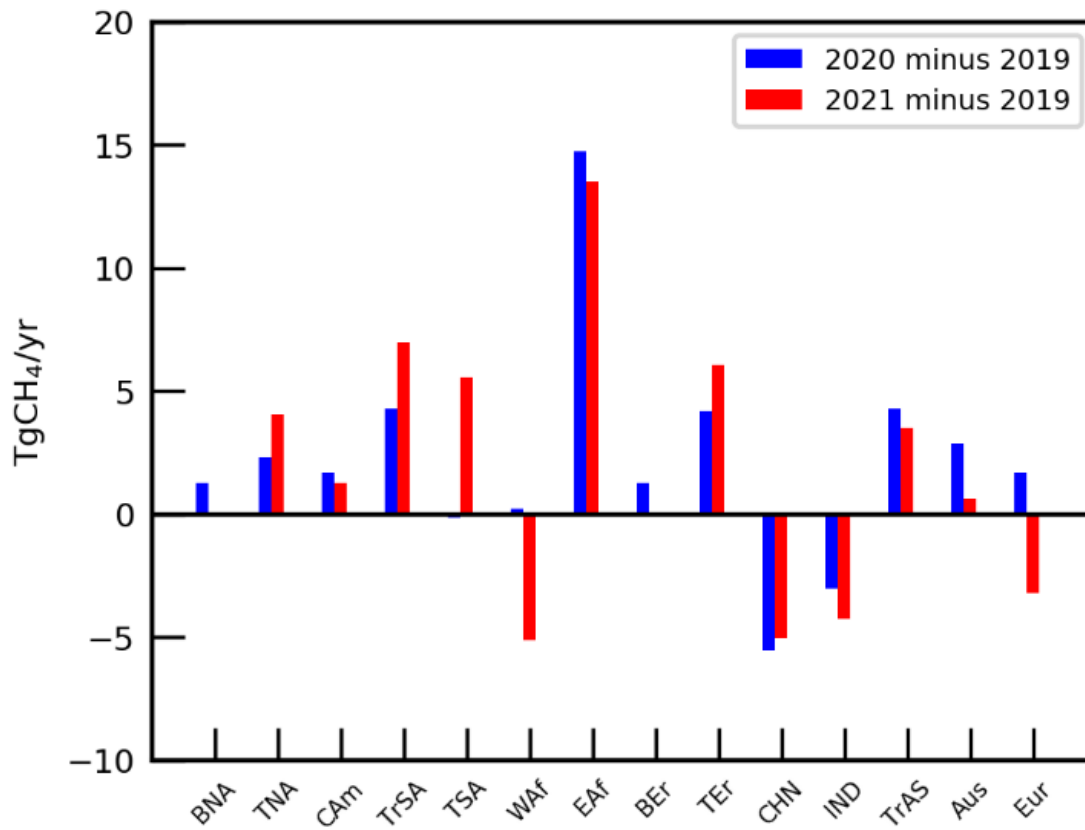


480 **Figure A5** Scatter plot of monthly GRACE-FP LWE anomalies (cm) and methane flux anomalies, 2018-2021, over a) Tropical South America, b) Eastern Africa, and c) Tropical Asia. Red lines denote the linear regression. Numbers atop of each panel denote the Pearson correlation coefficient r and the p-value.



485

Figure A6 Global *a posteriori* emissions of methane (g/m²/yr) inferred from GOSAT methane column data for 2020 (panel a) and 2021 (panel b).



490 **Figure A7** As Figure 1b but for an inversion that uses GOSAT proxy XCH₄ and *in situ* methane data.

Appendix B: Description of box model calculation

495 To calculate global emissions of methane from the NOAA global mean data we use a simple one-box model. In this model, the change in global mean methane concentration over time is given by:

$$\frac{dB}{dt} = Q - kB$$

where B is the atmospheric mass of methane in Tg, k is the loss rate given as 1/lifetime and Q is the emissions rate. From this, after integration, the annual emissions rate can be calculated as:

500

$$Q_t = \frac{k(B_t - B_{t-1} \cdot e^{-k})}{(1 - e^{-k})}$$

505 The loss rate was tuned to match a steady state concentration of 1775 ppb during 2000-2006 based on constant emissions of 530 Tg yr⁻¹ during this period. We calculated the rolling 12-month annual emissions to track the progression of global emissions between 2019 and 2021. We used the difference between the atmospheric concentration in January 2019 and January 2020, February 2019 to February 2020, etc. to calculate the change in emissions in the intervening 12 months. Figure B1 shows the increase in emissions throughout 2020 followed by more variable month-to-month changes in 2021. The large increase in emissions primarily occurs in 2020, with emissions at the 12-month period ending in Dec 2020 being 27 Tg yr⁻¹ larger than the emissions one year earlier. In contrast if emissions are calculated using annual mean concentrations, it appears as if there is a larger emission increase in 2021. The box model results show that the highly simplified calculation based on global average data is consistent with the more complex inverse modelling approach applied to the GOSAT data.

510

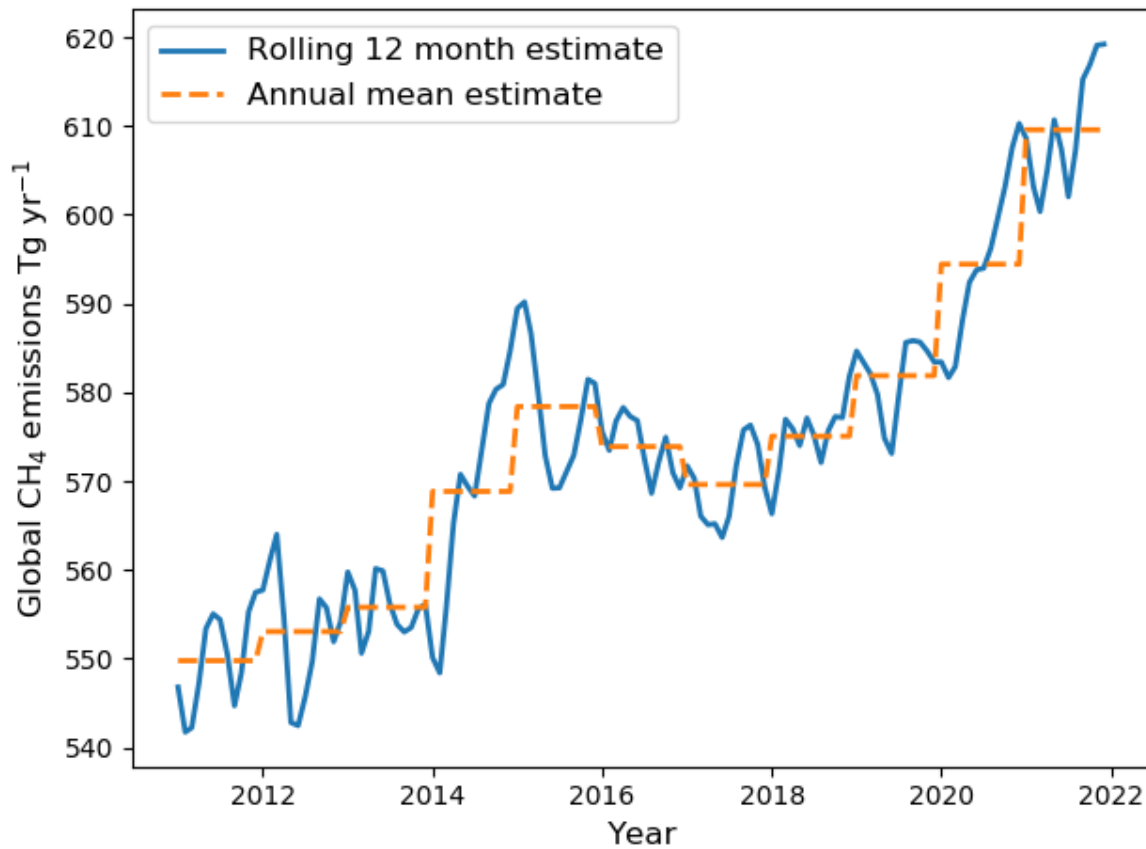


Figure B1 Global box model methane emission estimates between 2011 and 2021, respectively. Emission estimates are based on NOAA global mean surface data. The blue line denotes the rolling 12-month annual emissions, and the orange line denotes the emissions based on annual mean concentrations.

Appendix C: Evaluation of *a posteriori* flux estimates

We indirectly evaluate our *a posteriori* methane fluxes by comparing the GEOS-Chem methane distribution, driven by the *a posteriori* fluxes, with independent XCH₄ retrievals from Total Carbon Column Observing Network (TCCON) of Fourier transform spectrometers (Wunch et al., 2011). We use bias-corrected TCCON XCH₄ data from the latest GGG2020 public release of the TCCON data set from 2019 to 2021, including updates until October 2022. For a comprehensive description of the network and the available data from each TCCON site, we refer the reader to the TCCON project page. Here we use a subset of available TCCON data, dependent on their availability between 2018 and 2021 (Buschmann et al. 2022; De Mazière et al. 2022; García et al. 2022; Hase et al. 2022; Kivi, Heikkinen, and Kyrö 2022; Liu et al. 2022; Morino, Ohyama, et al. 2022b; Morino, Velasco, et al. 2022; Morino, Ohyama, et al. 2022a; Notholt et al. 2022; Petri et al. 2022; Pollard, Robinson, and Shiona 2022; Warneke et al. 2022; Shiomi et al. 2022; Té, Jeseck, and Janssen 2022; Wennberg, Wunch, et al. 2022; Wennberg, Roehl, Wunch, Blavier, et al. 2022; Wennberg, Roehl, Wunch, Toon, et al. 2022; Wunch et al. 2022; Zhou et al. 2022). For further details about the data we direct the reader to the TCCON project page: <http://tccondata.org/>.

Figure C1 shows the mean and standard deviation of the differences between our *a posteriori* model simulation and TCCON GGG2020 data in 2019 and 2020. The *a posteriori* model simulation is driven by our *a posteriori* methane emission estimates. We sample the associated model 3-D atmospheric methane distributions at the time and location of each TCCON site used. We then convolve the sampled vertical profile with site- and time-dependent TCCON instrument averaging kernels, which describes the altitude-dependent instrument sensitivity to changes in atmospheric methane concentration.

We do not report results for 2021 due to data availability; for data that are available, we find the mean statistics (not shown) are similar to those we report here for 2019 and 2020. For most sites, we find the mean bias is typically smaller than ± 10 ppb and the standard deviation has a range 5-15 ppb with typically values smaller than 10 ppb. We find the largest differences at northern high latitudes where the model has a large overestimate (~ 10 ppb), consistent with previous studies (Feng et al., 2017, 2022), due to poor coverage of GOSAT data during the boreal winter and to model error.

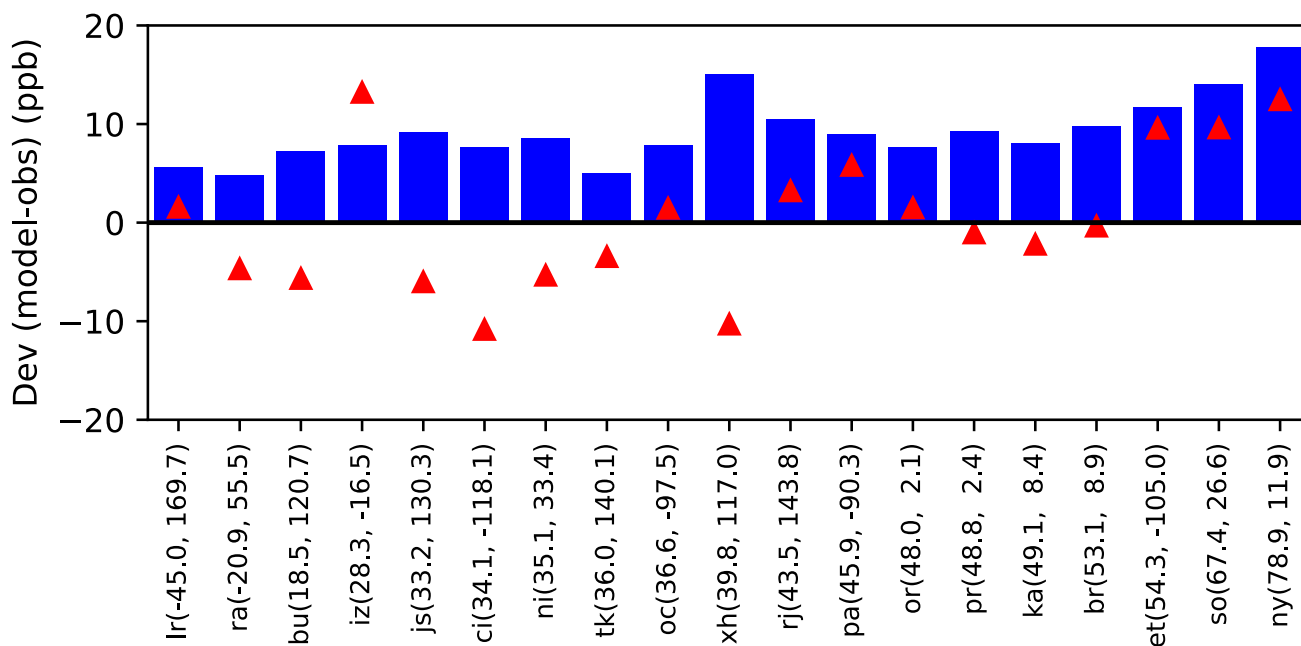


Figure C1 Statistical comparison of the GEOS-Chem *a posteriori* methane distribution and TCCON XCH₄ data (v GGG2020) in 2019 and 2020. Red upward triangles denote the mean bias and the blue bars denote the corresponding 1s values.

540

Appendix D: Time-dependent OH reduction sensitivity test

We assume a temporal-spatial distribution to describe the OH reduction in 2020, following a recent study on tropospheric ozone changes in 2020 and 2021 (Ziemke et al., 2022). First, we divide the world into regions: northern hemisphere (20°N-90°N) and the rest of the world. We assume the reduction in OH in the northern hemisphere starts from the boreal Spring of 2020 and peaks during the summer with a magnitude of 9% (blue line, Figure D1), higher than the ozone reduction found by Ziemke et al. (2022). For latitudes south of 20°N the time evolution of the reduction in ozone is less clear (Ziemke et al., 2020). We assume for simplicity that the OH reduction at these latitudes (red line, Figure D1) has a smaller peak value (-2.3%) and with a time lag of one month compared to the northern hemisphere region.

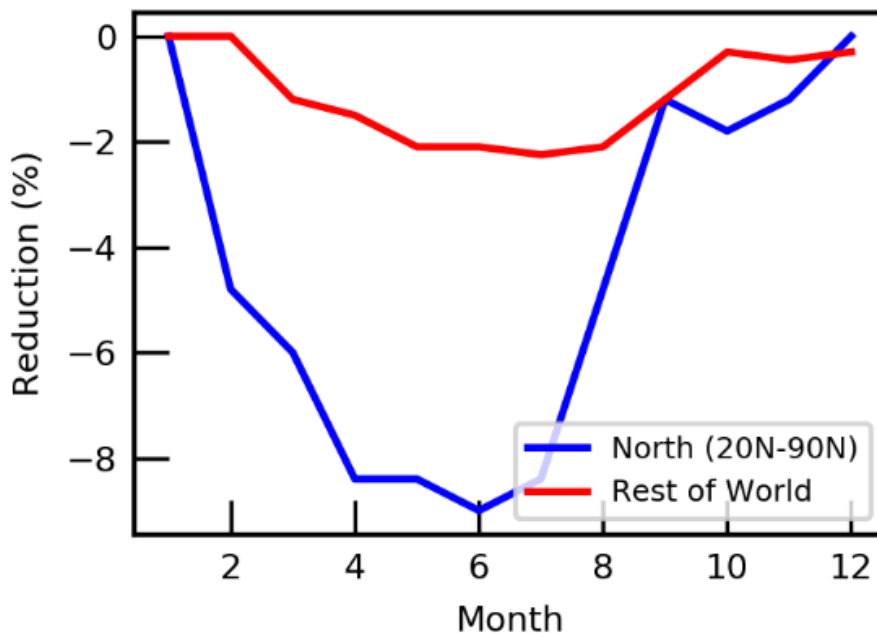


Figure D1 Assumed temporal distribution for OH reduction (%) in the northern hemisphere (20°N-90°N, blue line) and the rest of the world (red line) for our sensitivity calculation.

Our inversion that uses this assumed time-dependent OH reduction results in an annual global methane emission of 602.2 ± 11.2 Tg for 2020, which is about 8.5 Tg (~30%) smaller than our control run that used a fixed OH climatology (Table 1). This is consistent with increased methane emissions being primarily responsible for the anomalously large atmospheric growth rate of methane in 2020. We find that introducing an additional localized 25% OH reduction over China in March 2020 reduces the *a posteriori* global methane emission increase (Table 1) by only 0.26 Tg.

Appendix E: Atmospheric OH inversion

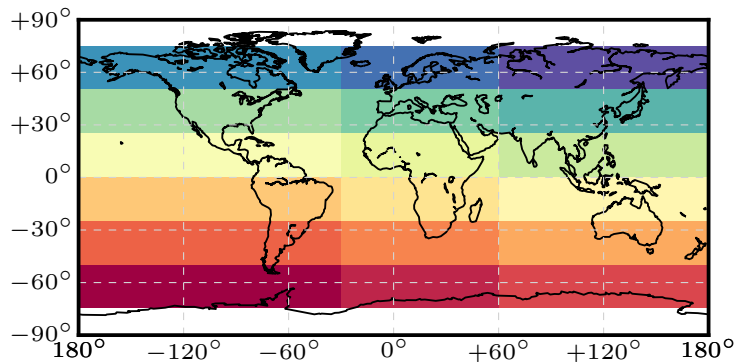
Currently there is no direct observation of the global distribution of atmospheric OH. Indirect constraints on atmospheric OH from the changing lifetimes of trace gases such as CO and methane are insufficient to infer determine 3-D distributions of OH.

560 Here, as part of the state vector, we infer 18 scaling factors for monthly *a priori* OH fields from atmospheric methane observations (section 2). These scaling factors correspond to 18 geographic regions (Figure E1). We define six 25° latitude bands between 75°S and 75°N. We do not consider scaling polar OH values. We then split each of latitude band into three longitude ranges, chosen so that each region contains a different tropical land mass: -180° to -30°; -30° to 60°; and 60° to 180°.

565 The Jacobian matrix, which describes the sensitivity of model methane concentrations to regional OH fields, is calculated with GEOS-Chem forced by *a priori* methane fluxes from the control run (Table 1) but with the OH climatology reduced by 5% for each of the 18 regions. To reduce the computational cost of this calculation, we use the same four-month lag window for the OH scaling factor estimates as for the methane emission estimates. So that each monthly OH scaling factor will be constrained only by observations in the subsequent four months, but its impact will remain for the entire experimental period. We used the OH climatology as our *a priori*, and assume a uniform 5% uncertainty for each of the 18 regions so that the 2-sigma range covers possible OH changes that range $\pm 10\%$. We use such a simple linearization scheme to adjust surface methane emissions and the monthly tropospheric OH by optimally fitting model calculations to atmospheric methane observations.

570 We conduct the joint inversion for 2018 to 2021, including the 18 monthly OH scaling factors and methane emissions, and use the same atmospheric methane data used by the control calculation. The corresponding methane emissions estimate in 2019 is now 606.8 ± 13 Tg/yr, about 23.1 Tg/yr higher than the control run. This higher emission is a result of (and largely cancelled out by) an elevated tropospheric OH loss of methane of 24.5 ± 8 Tg/yr, which is simultaneously inferred from the observation datasets. As expected, the resulting *a posteriori* atmospheric methane field is consistent with the assimilated GOSAT data and with independent TCCON observations (Figure D2). Further work is required to assess whether the higher methane loss is due to errors in the OH climatology or errors in atmospheric methane corresponding to the *a priori* inventories.

580 The global *a posteriori* methane emission estimate for 2020 is also higher than the control run (627.3 ± 13 Tg/yr vs 610.7 ± 11.3 Tg/yr), but the 17 Tg/yr increase is smaller than for 2019. As a result, the increase in emissions from 2019 to 2020 is 20.5 Tg/yr, which is about 75% of the control run. The corresponding additional OH loss of methane in 2020 is about 8 Tg/yr smaller than in 2019, which we believe is due primarily to the OH reduction in 2020. These results are consistent with our sensitivity calculations that used a perturbed OH distribution (Appendix D).



585 **Figure E1** Definition of the 18 regions for OH scaling factors that we include in our joint OH factor-methane emission state vector.

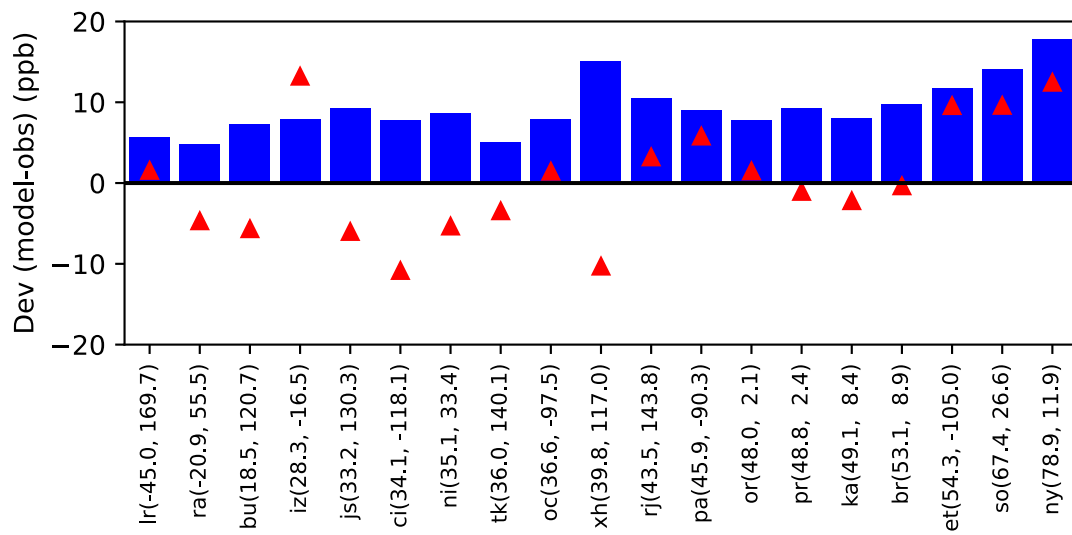


Figure E2 The same as Figure C1 but for the inversion that also includes OH scaling factors.